Applied Surface Science 609 (2023) 155250

Contents lists available at ScienceDirect

Applied Surface Science

journal homepage: www.elsevier.com/locate/apsusc

Full Length Article

Enhanced oxidization and corrosion resistance of silver nanowire based transparent conductor by nickel electroplating to obtain power conversion efficiency > 18 % in perovskite solar cells

Zhiqiang Shi [a], Shuyue Wu [a], Siyuan Lin [a], Jia Sun [a], Han Huang [a], Deming Kong [a], Yongli Gao [b], Conghua Zhou [a,*]

[a] Hunan Key Laboratory of Super-microstructure and Ultrafast Process, Hunan Key Laboratory of Nanophotonics and Devices, School of Physics and Electronics, Central South University, Changsha, Hunan 410083, China
[b] Department of Physics and Astronomy, University of Rochester, Rochester, NY 14627, USA

ARTICLE INFO

Keywords:
Corrosion
Roughness
Nickel
Electroplating
Stability
AgNWs

ABSTRACT

Silver nanowire based transparent conductor is expected to be widely used in optoelectronic devices. However, when used in perovskite solar cells, it suffers from heavy corrosion caused by the lead halide hybrid perovskite. To solve the problem, nickel electroplating is used to modify the transparent conductor in this study. It is observed that nickel electroplating not only improves the conductance, but also upgrades the corrosion resistance and the oxidization resistance of the transparent conductor. In addition, SnO_2 quantum dots are applied to flatten the conductor surface, while ITO sputtering is used to further improve the film conductance. After that, perovskite solar cells are fabricated on the modified transparent conductors. Current-voltage curves scanning under simulated irradiation shows that, power conversion efficiency of 18.37 % is achieved. Transient photocurrent / photovoltage decay curves and impedance spectroscopy tests show that, nickel treated transparent conductors could ensure efficient charge-extraction process, while retard charge recombination. Storage-stability of the devices is monitored, 80 % of initial performance is reserved after storage in dark for 432 h. The study paves the way for the application of silver nanowire basing transparent conductor in devices when heavy corrosion is involved.

1. Introduction

Perovskite solar cells (PSCs) have attracted ever-broadening attention during the past years. Due to the improvement on light absorption layer, charge-transport layer and also the interfaces between them [1–7], the photo-to-electric power conversion efficiency (PCE) has risen rapidly, from the initial 3.8 % to recorded 25.7 % [8–9]. One of the key merits of the PSCs lies on the lead-halide hybrid perovskite material, owing to the adjustable bandwidth, long carrier diffusion length, simple production process and the low price [10–14]. However, such perovskite material is highly corrosive to metal material (like Ag and Al) [15–16], which deteriorates device stability, and hinders the selection of electrode materials. For example, when using silver film as top electrode, the beneath charge-transport layer must be compact and continuous, so as to prevent the contact between perovskite and top electrode [17–19]. In fact, the top electrode could be well replaced by carbon material, which renders a branch of carbon-electrode basing PSCs [20–21]. However, as for the bottom electrode, it has long relied on metal oxide basing ones, such as ITO or FTO. It is well-known that relatively high temperature is needed during the preparation process of such oxide transparent conductor (TC), thus increasing the cost. On the other hand, these oxide TCs are fragile, also hindering the processing of light PSCs for portable electronic devices [22–24]. Therefore, it is necessary to explore new types of TCs that are compatible with both low temperature process and flexibility. In fact, several candidates have been developed, including graphene [25,26], metal mesh [16], carbon nanotubes [27], highly conductive PEDOT [23] and so on. Besides, silver nanowire (AgNW) based TC has also been developed, due to the excellent optoelectronic performance, mechanical flexibility [28,29], and the convenience of large-scale production [30–32].

During the past few years, AgNW TCs have been used as bottom electrodes for organic solar cells [33], and organic light emitting diode [34,35], and excellent performance has been achieved. Accordingly, one may also expect the usage of AgNW TCs in PSCs, but unfortunately, they

* Corresponding author.

https://doi.org/10.1016/j.apsusc.2022.155250
Received 10 August 2022; Received in revised form 3 October 2022; Accepted 7 October 2022
Available online 12 October 2022

suffer from heavy corrosion caused by the perovskite material. To deal with this problem, the corrosion resistance of these TCs should be largely improved. Indeed, several methods have been developed during the past few years. For example, in 2018, Liu *et al.* modified AgNW TC by graphene and obtained PCE of 13.36 % in flexible PSCs [24]. Miao *et al.* modified AgNW TC by polyimide, and prepared flexible PSCs with PCE of 11.8 % [36]. But for both of the two works, device stability was not reported. PEDOT:PSS (PH1000) was used to modify Ag-grid, and helped to prepare PSCs with PCE of 14.52 %. However, it was seen to corrode Ag-grid due to its acidic nature and the redox reaction, which caused heavy decay in PCE (drop by 20 % within 24 h) [16]. Besides, Tang *et al.* protected AgNW by sol–gel derived ZnO and atomic-layer-deposited TiO_2, and prepared flexible PSCs with PCE of 17.11 %, but again, the PCE dropped by 20 % in the first 24 h, even by 70 % within 50 h [37]. From above studies one can see that, corrosion has become a key issue that retards the application of AgNW TC in PSCs. To solve this problem, more efficient strategies should be explored.

Nickel film was previously used in PSCs and less reaction was observed between it and the perovskite material [38]. Recently, nickel was used to prepare copper-nickel alloy and used as top electrode for PSCs, which benefited device stability [39]. Nickel electroplating was also used to modify AgNW TCs [40], which improved conductivity and corrosion resistance of the TCs. In 2020, with the help of Ni-electroplating, Cho *et al.* prepared perovskite nanoparticles basing light-emitting diodes on AgNW TCs [41]. However, such strategy has less been applied in PSCs. To make possible usage in efficient and stable PSCs, here in this article, a Ni electroplating involved three-step modification strategy is proposed. At first, a thin layer of metal nickel is electroplated on the surface of AgNWs; Secondly, SnO_2 quantum dots (SnO_2 QDs) are imported to fill the voids between nanowires; At last, thin layer of ITO is sputtered on top. Then the modified TC is used as bottom electrode. The surface morphological properties and the opto-electronic performance of the transparent conductors are examined after each step modification. Effect of the modification on the power conversion properties of PSCs is carefully examined.

2. Experimental section

2.1. Materials and regents

Silver nanowires precursor (AgNWs, 99.5 %) were purchased from Aladdin. 2, 2′, 7, 7′- tetrakis [N, N-di (4-methoxyphenyl)amino] - 9, 9′ -spirobifluorene (spiroOMeTAD, 99.86 %) was from Advanced Election Technology. Lead iodide (PbI_2, 99.99 %), formamidinium iodide (FAI, 99.5 %), methylammonium bromine (MABr), and methylammonium chlorine (MACl, 99.5 %) were bought from Xi'an Polymer Light Technology Corp. Anhydrous N, *N*-dimethylformamide (DMF, 99.9 %), dimethyl sulfoxide (DMSO, 99.8 %), polymethylmethacrylate (PMMA, average Mw ≈ 350 000), chlorobenzene (CB, 99.8 %), 4-*tert*-butylpyridine (4-TBP, 96 %), and bis (trifluoromethane) sulfonamide lithium salt (Li-TFSI) were bought from Sigma. Boric acid (H_3BO_3, 99.5 %), ethylenediamine hydrochloride ($C_2H_{10}Cl_2N_2$, 99 %), nickel (II) chloride hexahydrate ($NiCl_2{\cdot}6H_2O$), acetonitrile (AC, 99.8 %), tin (II) chloride dehydrate ($SnCl_2{\cdot}2H_2O$, 98 %), ethanol (99 %), acetone (99 %), and isopropyl alcohol (IPA, 99 %) were purchased from Sinopharm (Shanghai). ITO target was bought from Beijing GoodWill Metallic Technology.

2.2. Preparation of AgNW TC and the modification

Before deposition of AgNWs, glass slides were ultrasonically cleaned in deionized water, acetone, deionized water, IPA each for 20 min, then dried in oven and further treated by UV/Ozone for 20 min. AgNW TCs were prepared by spin-coating AgNWs precursor on glass slide (2000 rpm), being followed by annealing at 100 °C for 30 min in glove box filled with nitrogen. Modification was done by three steps: i) Thin layer nickel was electroplated on AgNWs using current of 15 mA for ~ 10 s. Digital source-meter (model 2400, Keithley) was used as the current-source. Electroplating solution with 1 mol/L $NiCl_2$, 0.5 mol/L H_3BO_3, 0.5 mol/L ethylenediamine hydrochloride was prepared in deionized water. Before electroplating, oxygen was expelled from the solution by nitrogen gas bubbling for 20 min. After nickel electroplating, the TC film was annealed at 100 °C for 30 min in vacuum oven. ii) SnO_2 layer was deposited on nickel coated TCs by spin-coating SnO_2QDs solution (0.1 mol/L) at 3000 rpm for 30 s, followed by annealing at 150 °C for 60 min in air. iii) Thin layer of ITO (~60 nm in thickness) was sputtered to further upgrade the optoelectronic performance of the AgNW TCs. SnO_2 QDs were prepared by dissolving $SnO_2{\cdot}2H_2O$ in mixed solvents between ethanol and deionized water, with volume ratio of 5:1. It was stirred for 48 h before usage and the concentration was adjusted to be 0.1 mol/L. ITO sputtering was done in PECVD (TRP450, SKY TECHNOLOGY DEVELOPMENT CO., Ltd. CHINESE ACADEMY OF SCIENCES), with Argon gas pressure of 0.6 Pa, and sputtering power of 50 W.

2.3. Assembly of PSCs

Before assembly of PSCs, the obtained AgNW TCs were ultrasonically cleaned in deionized water, IPA each for 10 min, dried in oven, and further treated by UV/Ozone in air for 10 min. SnO_2 layer was coated on the TCs by spin coating the SnO_2 quantum dots precursor by speed of 3000 rpm for 30 s, being followed by annealing at 150 °C for 60 min in air and further treated by UV-Ozone for 20 min. Perovskite layer was prepared as following. Firstly, PbI_2 solution (1.2 mol/L in mixed solvent between DMF and DMSO with volume ratio of 9.5:0.5) was spin-coated (2000 rpm, 30 s) on SnO_2 film and annealed at 70 °C for 5 min in nitrogen. Secondly, mixture solution of (FAI: MABr: MACl = 60 mg: 6 mg: 8.2 mg, dissolved in 1 mL IPA) was spin-coating (2000 rpm, 30 s) on top of the PbI_2 film, being followed by annealing at 145 °C for 20 min in air (RH≈ 35 %). This led to perovskite with possible formation of $FA_xMA_{1-x}Pb(Cl_yBr_{1-x-y}I_x)_3$. Then hole-transport layer was prepared by spin-coating SpiroOMeTAD solution at 3000 rpm for 30 s on top, followed by annealed at 85 °C for 5 min in nitrogen [19]. The spiroOMeTAD solution was prepared by dissolving 72.5 mg SpiroOMeTAD powder in 1125 μL CB. 250 μL PMMA solution (0.48 mol/L, in CB), 18 μL Li-TFSI solution (1.81 mol/L, in acetonitrile), 29 μL 4-tBP were added as additives. Finally, silver film (~100 nm) was thermally evaporated to serve as the top electrode.

2.4. Material characterization and device performance evaluation

UV–Visible transmittance spectrum of transparent conductors and PVSK films were measured by UV–vis spectrophotometer (TU-1800). To reflect the transmittance of the coated films on substrate, similar substrate is chosen as the reference. As such, a baseline is recorded by testing the transmittance of glass (or the substrate) in wavelength range of 300 ~ 1100 nm. Sheet resistance of transparent conductors was measured using four-point probe method (SDY-4D). Morphological properties of AgNWs based composite TCs, the surface and cross-sectional images of PVSK were characterized by atomic force microscope (AFM 5500, Agilent Technologies) and scanning electron microscopy (SEM, FE-SEM, MIRA3 LMU, TESCAN, equipped with EDS affiliate). Morphological properties of AgNWs are monitored by transmission Electron Microscope (TEM, Tecnai G2 F20, equipped with EDS affiliate) respectively. X-ray diffraction (XRD) (Advance D8 Bruker, Empyrean Alpha 1) was used to characterize the crystallization AgNWs of PVSK films. Photoluminescence (PL) of PVSK films was measured by Spectro-fluorimeter (F-4700, Hitachi). Current-voltage characteristics of perovskite solar cells were recorded by digital source-meter (model 2400, Keithley) under simulated illumination (AM1.5G, 100 mW/cm^2, Enlitech SS-F7-3A). The intensity was calibrated by standard silicon cell (SRC-1000-TC-QZ-N, Enlitech). External quantum efficiency (EQE) was measured by spectrum performance testing system (7-SCSpec, Beijing)

with AC mode. Transient photovoltage / photocurrent (TPV/TPC) decay curves were obtained by a home-made system which consisted of a digital oscilloscope (DSO-X 3104A, Keysight) and N_2 laser (NL100, 337 nm, Stanford). During the TPV test, background open circuit voltage (V_{oc}) of about 1050 mV was generated by steady illumination, and laser pulse was imported to generate ΔV_{oc} of about 5 % of the background one. Impedance spectroscopy (IS) was conducted on electrochemical workstation (CHI 660D, Chenhua) under open circuit and dark condition, with frequency range of 0.1 Hz ~ 1 M Hz. The obtained curves were fitted by homemade software. In order to measure the storage stability, devices were kept in dark without encapsulation [ambient, with relative humidity of 30 (±5)%]. Periodic test was conducted to evaluate the storage stability.

3. Results and discussion

3.1. Effect of the modification on surface morphological properties and optoelectronic performance of AgNW TCs

AgNWs are coated on glass substrates by spin-coating. As shown in Fig. 1 (a) to (d), in order to improve the corrosion resistance and the surface smoothness of AgNW TCs, modification is performed by three steps: i) Step 1, nickel electroplating; ii) Step 2, SnO_2QDs coating; iii) Step 3, ITO coating. Nickel electroplating is used to improve corrosion and oxidization resistance of AgNW TCs due to the relative inert nature of metal Ni. SnO_2QDs are applied to fill the void between nanowires as to flatten the surface. ITO film is coated by magnetic sputtering, which increases the adhesion of nanowires on the substrate due to the high kinetic energy of sputtered particles by Ar^+ plasma. For the sake of the following presentation, bare AgNW TCs prepared on glasses are noted by "AgNW", while that modified by step 1 are marked by "AgNW/Ni", that by step 2 or 3 marked by "AgNW/Ni/SnO_2", and "AgNW/Ni/SnO_2/S-ITO", respectively.

Amongst these three steps, nickel electroplating focuses on the enhancement of the corrosion ability of AgNW itself, thus plays a key role. After electroplating, metal Ni is coated on AgNW due to the anode / cathode reaction [formulas (1) / (2)], respectively:

$$\text{annode reaction: } Ni - 2e^- = Ni^{2+} \quad (1)$$

$$\text{cathode reaction: } Ni^{2+} + 2e^- = Ni \quad (2)$$

According to the principle of electrochemistry, thickness of nickel layer will increase with current and time, according to formulas (3) and (4):

$$w = \frac{aA_{wt}Q}{nF}, \quad (3)$$

$$Q = It, \quad (4)$$

where w, a, A_{wt}, n, F, I and t represents ion mass of electrochemical reaction reduction, electroplating efficiency, relative atomic mass, reduction on ion valence, Faraday constant, electroplating current and time, respectively.

Scanning electron microscope (SEM) is used to monitor the effect of electroplating on surface morphological properties of the AgNW TC. Top view surface images and width distribution of AgNWs are shown in Fig. 1(f) and (g). After Ni electroplating, nanowires become thicker. Statistics show that the average nanowire width increases from 39.78 (±4.91) nm to 64.56 (±6.29) nm. Element analysis is also performed by EDS. From Fig. 1(e), one can see that Ni has been formed. The formation of nickel could also be reflected from TEM study. As is shown in Fig. 2 (a) to (c), the AgNWs are coated with thin layer of nickel. From the element mapping one can see that, nickel could almost cover the whole surface of the AgNWs. HRTEM images in Fig. 2 (d) to (f) depict the difference in the atom arrangement of Ag (core) and Ni (shell). In addition, the thickness of the nickel layer is about 10 ~ 20 nm, coinciding well with SEM test. As such, nickel layer has been formed on the surface of AgNWs by electroplating. This could protect AgNWs from corrosion, and then help the application in PSCs.

XRD characterization is performed using relative slow scanning rate (2°/min). From Fig. S1 it could be seen that, before Ni coating, two peaks of 38.0° and 44.4° appear, which is due to (1 1 1) and (2 0 0) of Ag (JCPDS04-0783), respectively; after Ni coating, two peaks at around 38.0° and 44.6° appear. In addition, intensity of peak at 44.6° becomes stronger than the peak at 38.0°, showing that new crystallographic phase forms. Careful examination shows that, these two peaks are belonging to crystal facets of Ag (1 1 1), and Ni (1 1 1) (JCPDS04-0850). Nickel oxide (NiO_x) has not been clearly detected due to the N_2 bubbling

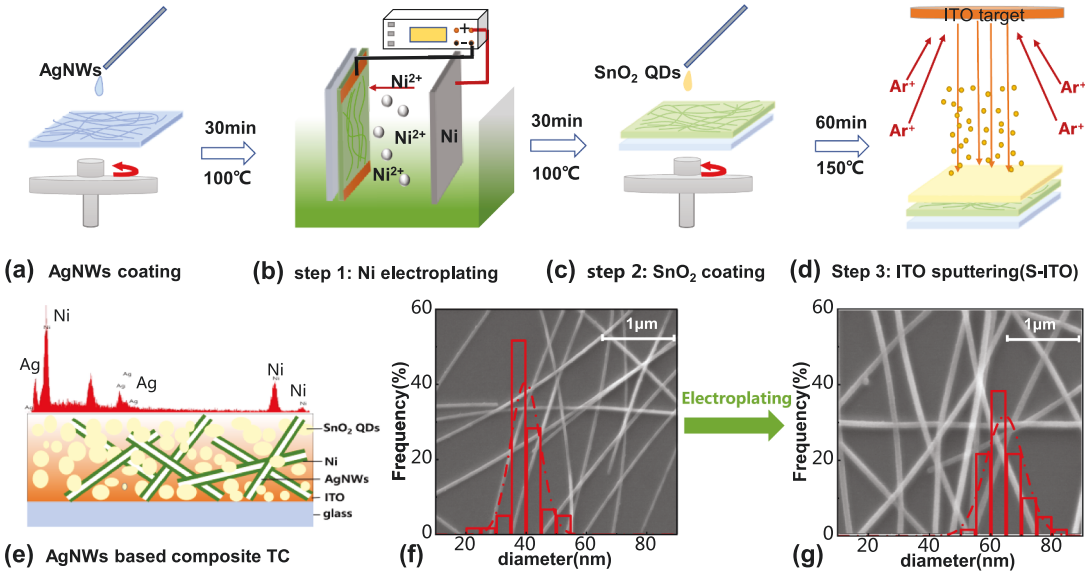

Fig. 1. Schematic of modification on AgNW TCs. (a) bare AgNW TC; (b) step 1: Ni electroplating; (c) step 2: SnO_2 coating; (d) step 3: ITO sputtering; (e) AgNW composite TC after 3-step modifications. Scanning electron microscope image of AgNW TC: (f) before, and (g) after Ni electroplating. Element analysis is shown on top of (e), while the diameter distribution of nanowires is shown by the red histograms that embedded in (f) and (g). (For interpretation of the references to colour in this figure legend, the reader is referred to the web version of this article.)

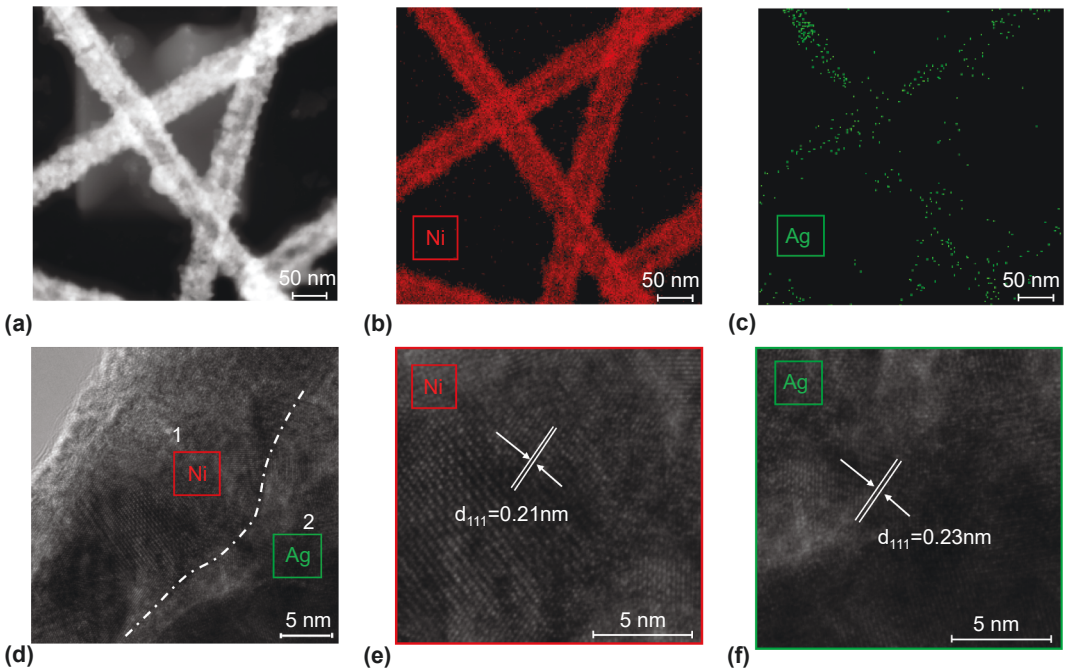

Fig. 2. (a) TEM image of AgNWs after nickel electroplating, and corresponding element distribution of: (b) Ni and (c) Ag. (d) HRTEM image of the AgNWs after electroplating, and enlarged region of: (e) Ni and (f) Ag.

and vacuum annealing techniques during the modification processes. Accordingly, electroplating has successfully deposited thin layer of nickel on silver nanowires. Such modification will increase the corrosion resistance of AgNWs which is beneficial for the application in PSCs.

Optoelectronic properties of AgNW basing TCs are studied by measuring the transmittance spectrum and the sheet resistance. Fig. 3 (a) shows typical transmittance spectra of the four samples. As expected, bare AgNW TC shows high transmittance (T%) at all the measured wavelength range of 300 ~ 1100 nm. The slight decrease at 350 nm is due to the absorption of surface plasma resonance [42]. After Ni electroplating, the whole spectrum moves down, due to the increased area fraction of nanowires (nanowires become thicker after electroplating). Besides, SnO_2 coating brings less effect to the transmission, though ITO coating causes relatively heavy absorption at wavelengths between 300 and 800 nm, especially for region between 300 and 500 nm. For easy comparison, T% at 550 nm is picked up from those spectra, and plotted in Fig. 3 (d). It is 97.72 % for bare AgNW TC, while 90.62 % after nickel electroplating. After SnO_2 coating and ITO sputtering, it decreases to 90.58 % and 81.66 %, respectively. As for sheet resistance (R_{sh}), it is 111.6 (±6.35) ohm/sq for bare AgNW TC, after Ni

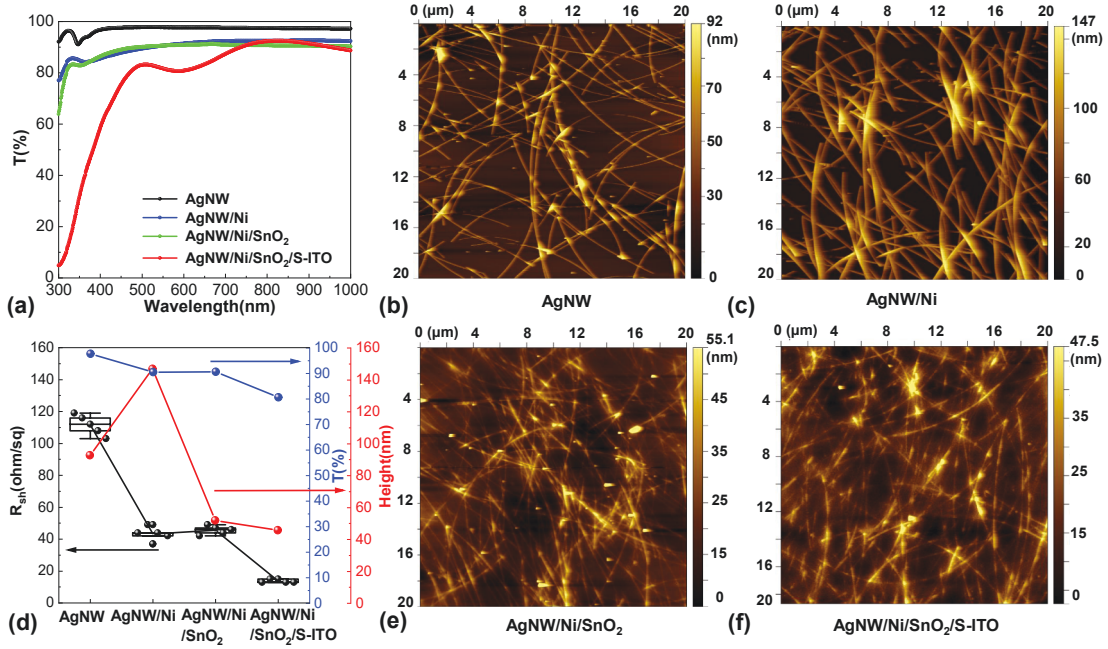

Fig. 3. (a) Effect of modification on UV–Visible transmittance properties (effect of glass has been subtracted). Typical atom force microscope images of TCs: (b) AgNW, (c) AgNW/Ni, (e) AgNW/Ni/SnO_2 and (f) AgNW/Ni/SnO_2/S-ITO. (d) Effect of modification on optoelectronic properties (R_{sh} and T%) and surface roughness (height difference) of AgNW TCs.

electroplating, it decreases to 43.2 (±4.32) ohm/sq. It changes little after SnO_2 coating because SnO_2 is semiconducting and less conductive than AgNWs. However, SnO_2 is a kind of efficient ETL that widely used in PSCs [43–44]. Anyway, R_{sh} further drops down to 13.8 (±1.10) ohm/sq after ITO sputtering. Clearly, Ni electroplating and ITO coating have made contribution to the film conductance. Effect of nickel thickness on the optoelectronic performance of the AgNW TC is examined by varying the electroplating time. As is shown in Fig. S2 (a), with electroplating time prolonging, both of the transmission (T%) and sheet resistance (R_{sh}) decrease. A figure of merit (FoM) is defined as the ratio between T % (@550 nm) and R_{sh}. As is shown in Fig. S2 (b), it increases with the electroplating time. For example, FoM is 0.876 for bare AgNW TC, after nickel electroplating for 8 s, it increases to 2.098, indicating that the photoelectric properties have been improved a lot after nickel electroplating.

Surface morphological properties are monitored by atom force microscope (AFM). Typical surface images are shown in Fig. 3(b), (c), (e) and (f). It can be seen that surface roughness of TC increases after electroplating. For example, the maximum height rises from the initial 92 nm to 146 nm, increasing by nearly 60 %. Such behavior is due to nickel coating, which adds to the width of the nanowires. After one layer of SnO_2 is coated, it decreases sharply to 50.3 nm, showing that, SnO_2QDs could fill the voids between nanowires, thus smooth the TC surface. Such feature is important for a substrate in optoelectronic devices. Besides, SnO_2 has been verified for many times as efficient electron-transport material. As such, SnO_2 coating is helpful for the application of AgNW TC as bottom electrode. Following that, the sputtered ITO layer could also flatten the surface, further reducing the height difference to 44.9 nm. Besides, the sputtered ITO layer (60 nm) itself shows sheet resistance of about 35.8 (±1.10) ohm/sq. This could make it conductive for the void part between nanowires, which is helpful for charge extraction and transport. For comparison, sheet resistance, T% (@550 nm), as well as the height difference of the AgNW TCs are all collected in Fig. 3 (d). One can clearly see that, Ni electroplating is beneficial for film conductance, SnO_2 coating is efficient in surface flattening, while ITO benefits the both, though the major contribution to the network conductivity is AgNW and Ni electroplating. Besides, Ni electroplating could improve the adhesion of AgNWs to substrate. As shown in Fig. S3, without electroplating, AgNWs could be easily peeled off by tape. After electroplating, adhesion is obviously strengthened. In addition, ITO sputtering could further improve the adhesion ability of AgNWs matrix on the substrate.

3.2. *Effect of modification on oxidization and corrosion resistance of AgNW basing TCs*

Aging properties of the AgNW TCs are studied by stress tests. To evaluate the corrosion resistance, sheet resistance (R_{sh}) is measured after each of the three-step modifications; meanwhile, surface morphological properties are monitored. The first stress test is UV / Ozone irradiation. In fact, UV / Ozone irradiation is applied frequently to clean ITO / FTO substrate before device preparation. Accordingly, AgNW TCs (whether modified or not) are treated by UV / Ozone irradiation in air for 10 min. As shown in Fig. 4 (a), without modification, R_{sh} increases from 110 ohm/sq to infinitely large, showing that the TCs turn to be insulating after the treatment. After Ni electroplating, R_{sh} remains almost unchanged, implying that the coated Ni metal has apparently increased the oxidization resistance. From the SEM images in Fig. 4 (b) and (c) one can see that, without Ni electroplating, small particles appear on AgNWs. Such phenomenon is similar to that reported before, showing nanowires have been oxidized [45]. However, after Ni electroplating is performed, such small particles could hardly be observed, indicating that Ni electroplating has improved the oxidization resistance against UV / Ozone treatment.

Another stressing test is MAI dipping. It is well-known that Ag could be corroded by lead halide perovskite, and the organic ionic salt that forms such perovskite [46]. As a result, it is essential to upgrade the corrosion resistance of AgNW TCs against perovskite materials. During the test, MAI solution (60 mg/mL in IPA) is casted on TCs, and kept in open air for 24 h. After that, the TCs are rinsed with IPA and dried, following which R_{sh} and surface morphologies are monitored. As shown in Fig. 4(d), without modification, R_{sh} increases from 110 ohm/sq to

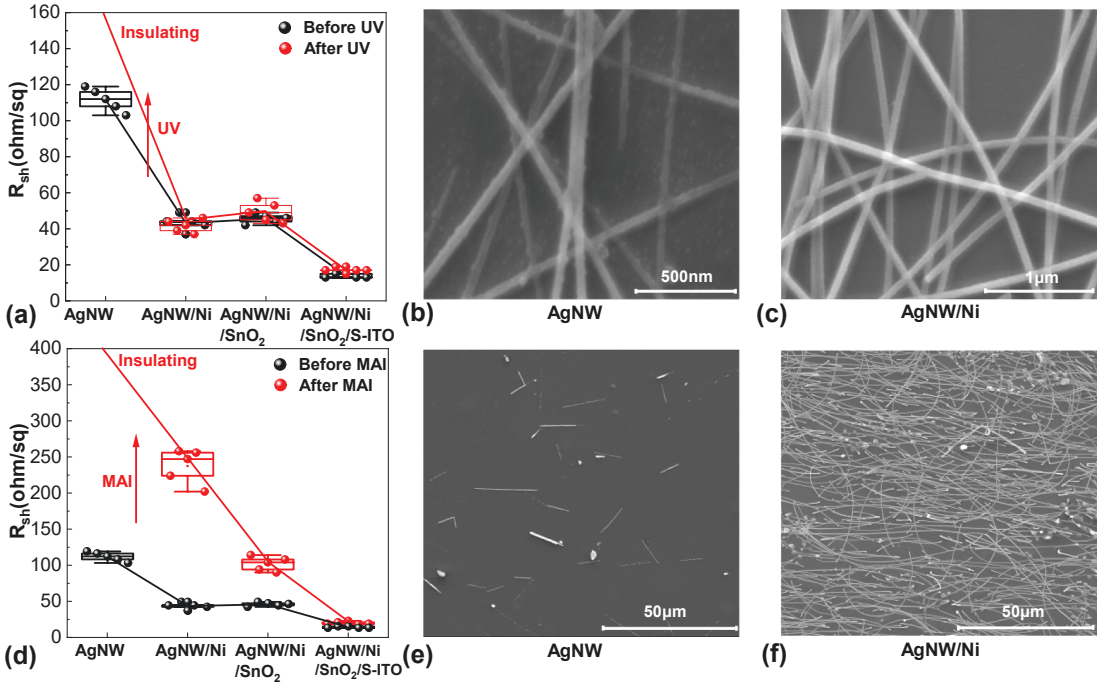

Fig. 4. (a) Comparison on sheet resistance of the four TCs before and after UV/Ozone irradiation for 10 min. (b) and (c) Typical SEM images of "AgNW" and "AgNW/Ni" after UV/Ozone irradiation for 10 min. (d) Comparison on sheet resistance of the four TCs before and after iodomethylamine (MAI) corrosion. (e) and (f) Typical SEM images of "AgNW" and "AgNW/Ni" after iodomethylamine (MAI) corrosion.

infinitely large, showing that the TCs turn to be insulating after MAI treatment. However, it increases from 43.2 to 237.4 ohm/sq after Ni electroplating, from 45.6 to 102 ohm/sq after SnO_2 coating, but changes little after ITO is sputtered. Such behavior shows that Ni-coating (15 mA for 8 s) could enhance the corrosion resistance, so is to SnO_2. However, adding one more layer of sputtered ITO could thorough upgrade the corrosion resistance. The improvement could be well-reflected from the SEM images [Fig. 4 (e) and (f)]. Without modification, most AgNWs have been etched off. However, for those nanowires modified by Ni electroplating, the majority could be left after MAI treatment. In fact, the corrosion reaction to AgNWs in wet air could be described by following formulas: [46]

$$CH_3NH_3I \xrightarrow{H_2O,\ O_2} CH_3NH_2 + HI \quad (5)$$

$$2HI + 2Ag \rightarrow 2AgI + H_2 \quad (6)$$

The improved corrosion resistance shows that, metal nickel is inert when facing the corrosive agents. In more, Ni coating could prevent the direct contact between such agents and silver, thus increasing the corrosion resistance. Similar protection could be provided by SnO_2 and ITO. However, ITO is suggested to be more efficient than SnO_2QDs, since it is more compact than the colloidal SnO_2 film. From the observations, one can see that, Ni-electroplating provides the first protection against corrosion, then the SnO_2 and ITO, this could also be reflected in the following studies on device.

3.3. Application in perovskite solar cells

According to above studies we know that the three-step modification helps to enhance the oxidization and corrosion resistences of the AgNW TC, while Ni electroplating plays the key role. As result, the modified AgNW TCs are used to fabricate perovskite solar cells (PSCs). For comparison, three more substrates are used, such as AgNW TCs with only SnO_2 and ITO modification (noted by "AgNW/SnO_2/S-ITO"), ITO sputtered on glass (noted by "S-ITO"), and commercial FTO. The sheet resistance and transmittance of different TCs are shown in Fig. S4. As shown in Fig. 5(a), perovskite grown on AgNW TC with 3-step modification shows similar crystallographic properties like that on FTO and S-ITO. Peaks at around 14.10°, 24.37°, 28.29° belong to the crystal plane (1 1 0), (2 0 2) and (2 2 0) of the α-phase perovskite basing on FA [47,48]. When AgNW TCs are only modified by SnO_2QDs and sputtered ITO, slight difference appears at 11.89°, 12.76°, which is due to crystal plane (0 1 0) of δ-phase perovskite, and crystal plane (0 0 1) of PbI_2 [49,50]. And the peak appears at 39.19° is due to AgI [51–53]. These three peaks are due to the reaction between perovskite and AgNW. For detailed comparison, XRD pattern is enlarged at the region near AgI. Without Ni electroplating, AgI is easier to appear. Besides, full-width at half magnitude (FWHM) of peak (1 1 0) is collected for the perovskite. As shown in Fig. 5, perovskite grown on Ni-modified AgNW TC comes out with FWHM of 0.104°, which is close to that grown on FTO, but smaller than that grown on the other kinds of substrates. As a result, Ni electroplating could improve the corrosion resistance, which benefits the growth of pervoskite crystallites.

Morphological properties of these perovskite films are monitored. As shown in Fig. 5 (e) to (h), pin-holes are seen for film grown on substrate of "AgNW/ SnO_2/S-ITO/SnO_2", while the other three cases all come out with smooth and compact surface. Optical properties of the perovskite films are measured. As shown in Fig. 5 (d), when AgNW TC is not modified, perovskite comes out with relative lower absorbance. Photoluminescence (PL) is also monitored. Thus the PL spectrum is not only affected by the crystalization of perovskite, but also by the interfacial charge-extraction process. For example, for perovskite grown on "FTO/SnO_2" and "AgNW/Ni/SnO_2/S-ITO/SnO_2", relatively lower intensity is observed for the PL peak at around 803 nm, while for that grown on "S-ITO/SnO_2" and "AgNW/SnO_2/S-ITO/SnO_2", relatively higher intensity appears. As stated above, the evolution in PL intensity is affected by both crystallization and charge extraction. Since perovskite films appear with similar crystallization for these four kinds of substrates, the relatively higher intensity might be due to the retarded charge-extraction. For example, sputtered ITO is less conductive than modified AgNW TC (by three steps), thus slower extraction is anticipated; while for AgNWs modified by SnO_2 and ITO, corrosion happens across the interface, this also slows down the extraction process.

PSCs with normal structure of "AgNW TC/SnO_2/perovskite/ spiro-OMeTAD/Ag" are prepared. Besides AgNW TC modified by three-steps, those modified by two-steps (without Ni electroplating) are also used as references. For comparison, commercial FTO and sputtered ITO (S-ITO) are also adopted. Cross-sectional SEM images of the four kinds of electrodes are shown in Fig. S5. For comparison, cross-section morphology is also examined on devices prepared on "AgNW/Ni/SnO_2/S-ITO", and commercial FTO, which are shown in Fig. S6. Typical current–density voltage (JV) curves are shown in Fig. 6(a). One can see that, without Ni

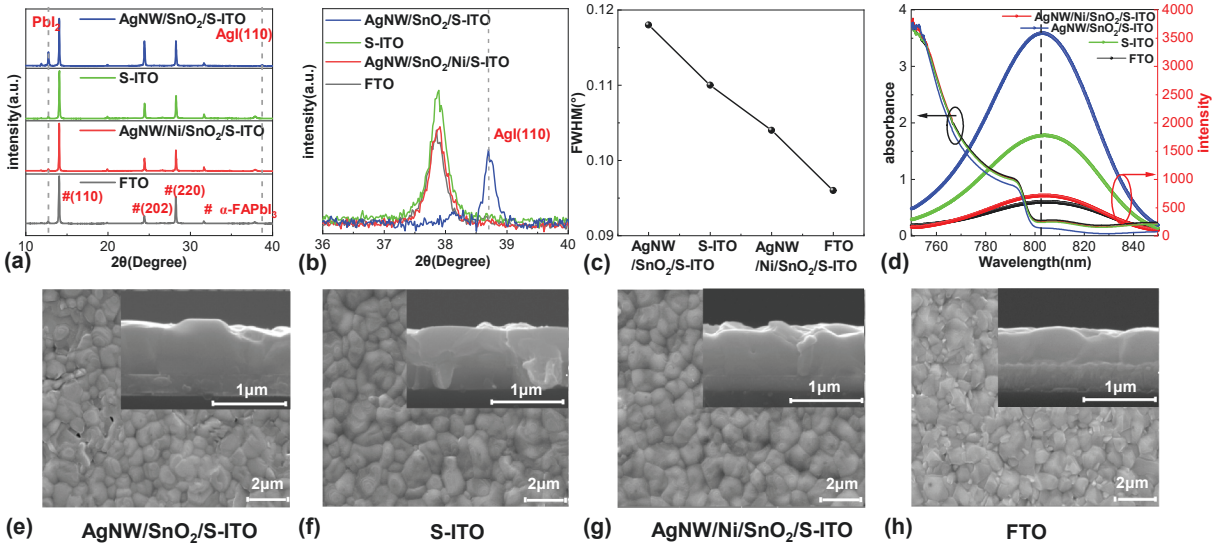

Fig. 5. (a) XRD patterns of perovskite films. (b) Enlarged part of XRD pattern of (a). (c) Full-width at half magnitude (FWHM) of the peak (1 1 0) for perovskite films. (d) UV–vis absorption and Photoluminescence (PL) of perovskite films. (e) to (h) Typical SEM images of perovskite films (inset shows cross-sectional SEM image of the same sample). Substrate information is noted in each figure.

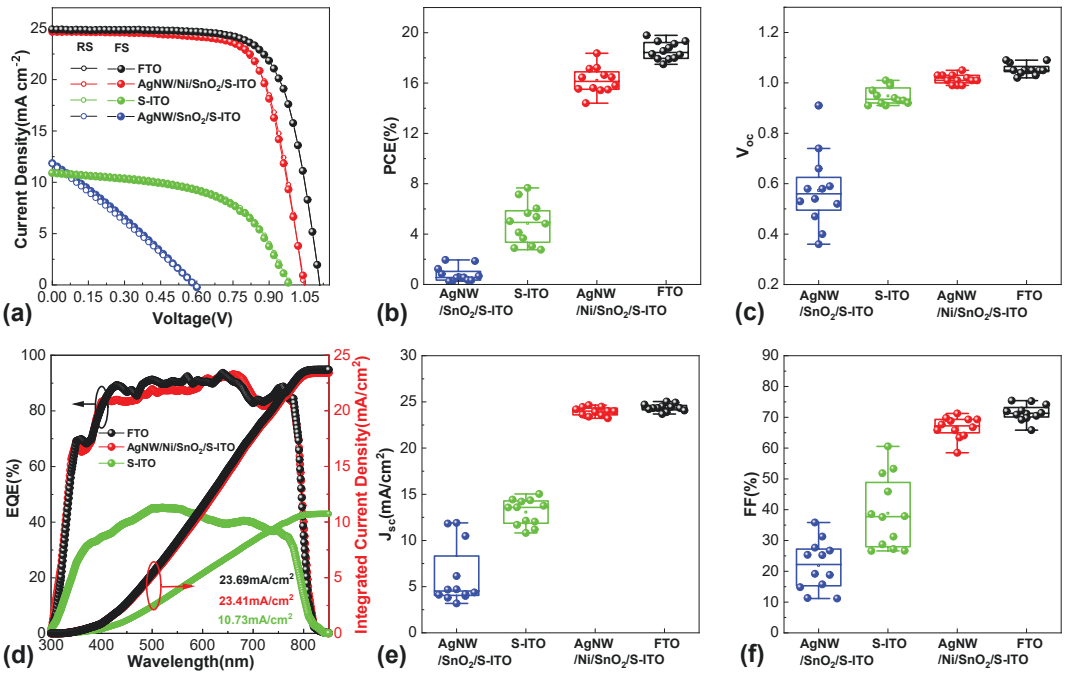

Fig. 6. (a) Typical current density–voltage (JV) curves ("RS / FS" represents reverse / forward scans, respectively). (d) Typical EQE spectrum and integrated J_{SC} of devices prepared on substrate of commercial FTO, "AgNW/Ni/SnO_2/ITO/SnO_2", and "S-ITO". Statistics on the performance parameters: (b) PCE, (c) V_{OC}, (e) J_{SC}, and (f) FF. All these parameters are picked from reverse JV scans.

electroplating, shunt behavior appears, this could also be seen in the dark JV curves (Fig. S7). While the other devices shows normal JV curves. Performance parametes relating to Fig. 6 (a) are collected in Table 1. As expected, without Ni-electroplating, poor PCE is recorded. After Ni electroplating, the PCE reaches 18.37 %, which is close to 19.79 % of PSC assembled on commercial FTO. The 7 % difference is mainly from the V_{OC} and FF, and partially from J_{SC}. Besides, sputtered ITO products relatively low PCE, mainly due to the larger sheet resistance. While for AgNW TC without Ni electroplating, very poor performance is recorded, which is due to the corrosion reaction between perovskite and AgNWs. Detailed comparison could be seen in Fig. 6 (b) to (f). Due to the improved oxidization and corrosion resistances, Ni electroplating makes all of the four performance parameters close to those basing on commercial FTO. Moreover, external quantum efficiency (EQE) spectra are shown in Fig. 6(d). Integrated J_{SC} of 23.69, 23.41 and 10.73 mA cm^{-2} are obtained, corresponding to 95.87 %, 94.96 % and 97.10 % of J_{SC} recorded from JV curves for PSCs assembled from modified AgNW TCs, and commercial FTO, respectively. Above observation clearly dispicts the potential application of Ni-modified AgNW TC in PSCs. It is worthy to note that, S-ITO itself harvests relative poor PCE (~6%), but after the incorporation with AgNWs, it could help to achieve higher PCE. As to the relative poor PCE, it is suggested to relate to two factors. The first one is the resistance, it could affect the charge-extraction and transportation (as will be reflected in TPC / TPV and IS studies). The second is the physicochemical properties of the surface of the S-ITO, it could affect the formation process of the halide perovskite film. However, it is anticipated that, better performance might be obtained after thorough surface modification could be made.

Table 1
Performance parameters of PSCs prepared on different substrates. Power conversion properties are measured under simulated irradiation (AM1.5G, 100 mW cm^{-2}).

Substrate	V_{oc}(V)	J_{sc}(mA/cm^2)	FF(%)	PCE(%)
FTO	1.096	24.71	73.08	19.79
AgNW/Ni/SnO_2/S-ITO	1.046	24.65	71.25	18.37
S-ITO	0.988	11.05	55.08	6.01
AgNW/SnO_2/S-ITO	0.592	11.91	27.69	1.95

Charge transfer and recombination dynamics of PSCs are studied by transient photocurrent / photovoltage (TPC/ TPV) decay curves, and impedance spectroscopy. Fig. 7 (a) and (b) present typical TPC / TPV decay curves for devices prepared on the four kinds of substrates. Charge-extraction time (t_d) and lifetime of photogenerated charge carries in PSCs (τ) are picked from the TPC / TPV by fitting. It could be seen that, t_d of devices prepared on "AgNW/Ni/SnO_2/S-ITO" is close to that of devices mounted on commercial FTO. While the other two kinds of substrate, or sputtered ITO (noted by "S-ITO") and AgNW TC without Ni electroplating, longer extraction-time is observed, implying slower charge-extraction process. The slower extraction process in S-ITO devices is due to the relative lower film conductivity of the substrate. While for substrate of AgNW TC without Ni electroplating, it might be relating to the corrosion reaction between AgNW and perovskite. Since corrosion will add to the defects across the interface, which lowers down the charge transfer rate due to the trapping / detrapping process [54]. As for the lifetime (τ), devices prepared on Ni containing AgNW TCs come with similar result like devices on FTO, while the other two kinds of devices show relatively smaller values. Similar behaivor is observed in impedance spectroscoy studies. Typical Nyquist plots of high-frequency region are shown in Fig. 7(d), those of low-frequency region are shown in Fig. S8. Charge transfer resistance (R_{ct}) and recombination resistance (R_{rec}) are obtained by fitting these plots to the equivalent circuits (shown in Fig. S9), [19] the results are shown in Fig. 7(e) and (f), respectively. It could be seen that, for both of these two resistances, PSCs on Ni treated AgNW TCs present similar values to those fabricated on FTO. While difference appears from other two cases. For example, "S-ITO" devices produce relatively larger charge transfer resistance (R_{ct}), while smaller recombination resistance (R_{rec}). Especially for devices prepared on non-Ni containing AgNW TCs, R_{rec} is ~ 100 Ω, comparing to ~ 10^7 Ω in the other three cases, showing heavy recombination happens. Relation between open-circuit voltage (V_{OC}) and light intensity is also examined. The result is presented in Fig. 7 (c), linear behaivor appears for both of the two kinds devices (modified AgNW TC and commercial FTO). In addition, the slopes are also close to each other.

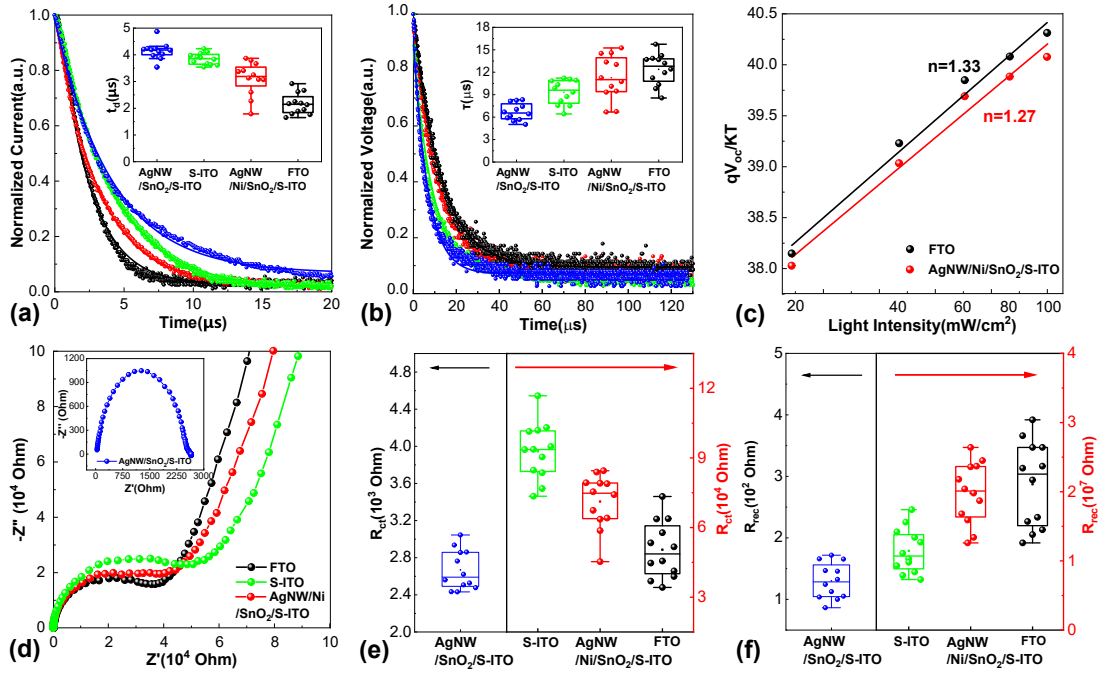

Fig. 7. (a) transient photocurrent (TPC) decay, and (b) transient photovoltage (TPV) decay curves of PSCs. (c) Plotting between qV_{OC}/K_BT and light intensity (presented in logarithm, or ln P); (d) Nyquist plots of high-frequency region to show the interfacial recombination resistance (R_{rec}) and charge transfer resistance (R_{ct}), respectively; (e) charge transfer resistance (R_{ct}), and (f) recombination resistance (R_{rec}) picked from the Nyquist plots.

Above observation shows that Ni electroplating could obviously hinder the corrosion reaction between AgNW and perovksite, which benefits the power conversion processes.

Photo-stability is examined by quasi maximum power point tracking (Q-MPPT, noting "quasi" is used here). As shown in Fig. 8(a), similar behavior appears between the two devices. Storage stability is also examined, the result is shown in Fig. 8 (b). A parameter of "T_{80}" is defined to record the time for device efficiency shrinks to 80 % of the initial value. To make meaningful comparison between current work and those previously published, and for detailed analysis, PCE and storage stability of PSCs (using AgNW TC as bottom electrode) are collected, and shown in Fig. 8(c) and Table 2, respectively. For example, Lu and coworkers modified AgNW TCs by graphene-oxide sheets in 2019, and obtained PCE of 9.62 % in PSCs, though the stability was not reported [58]. Tang *et al.* modified AgNWs by sol–gel derived ZnO and atomic-layer-deposited (ALD) TiO_2 in 2018, and prepared flexible PSCs with PCE of 17.11 %, but T_{80} was <24 h [37]. In 2020, Ko *et al.* prepared AgNWs TC with orthogonally arranged AgNWs and modified the network by PH1000, which helped to prepared a kind of ultrothin and flexible PSC with PCE of 15.18 % and T_{80} of 500 h [59]. However, Ma *et al.* also used PH1000 to modify the AgNWs TC, but observed relative poor stability (T_{80} of about 24 h), by which they ascribed to the possible corroison of PH1000 to AgNWs [16]. For current study, T_{80} of 432 h is obtained. The improved efficiency and stability is appealing for the application of AgNWs in PSCs. The prolonged stability is due to the improved corroision resistance by Ni electroplating, and partially by the sputtered ITO. Anyway, slight decrease is observed in Fig. 8 (b), which is due to the following two aspects: i) The uneven covering of Ni on AgNWs which makes it possible for contact between AgNWs and perovskite. Honestly, this could be reflected from the TEM images shown in Fig. 2. As a result, more studies are needed to improve the electroplating technique itself. ii) Decomposition of the perovskite layer itself, this could be reflected in FTO basing devices. However, the main cause of the PCE drop comes from the potential corrosion. This could be reflected by the ratio of PCE between devices basing on AgNW TC and FTO [Fig. 8 (b)]. As shown in Fig. S10, the flexible AgNW TC comes out with better flexibility than ITO based commercial flexible TC. The modification strategy is also efficient for AgNW TC grown on plastic (like PET) substrate. As such, flexible PSCs are also prepared, and an initial PSC of 9.2 % is observed. The problem mainly comes from the rough surface of

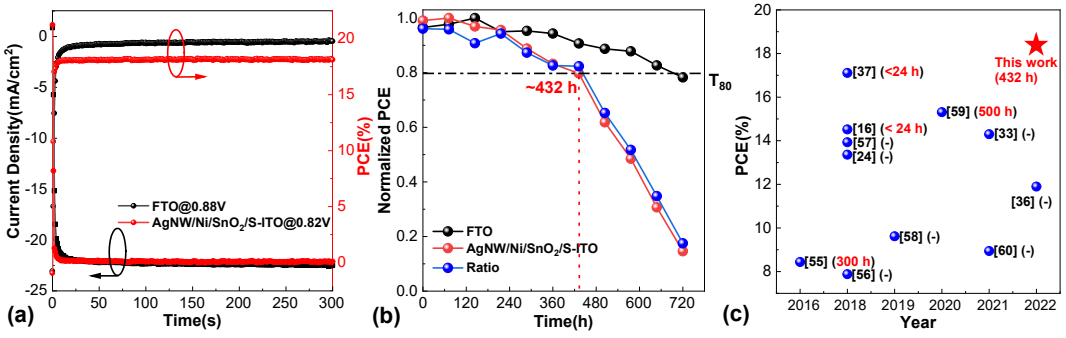

Fig. 8. (a) Quasi maxium power point tracking (Q-MPPT) of PSCs prepared on "AgNW/Ni/SnO_2/S-ITO" and commercial FTO. (b) Storage stability test of the PSCs based on "AgNW/Ni/SnO_2/S-ITO" and commercial FTO. Devices were stored in the dark (RH = 35 ± 5 %) and no encapsulation was used in all cases. (c) Typical PCE and storage stability of PSCs, picked from published literatures where AgNW basing TCs are used as bottom electrodes.

Table 2
Typical PCE and storage stability of PSCs, picked from published literatures where AgNW basing TCs are used as bottom electrodes.

Entry	Electrodes	Initial PCE (%)	T_{80}(h)	Year	Ref
This work	Glass/AgNW/Ni /SnO_2/ITO	18.37	432	2022	This work
1	Glass/ITO/AgNW /ITO	8.44	~300	2016	[55]
2	PEN/AgNW/ZnO /TiO_2	17.11	<24	2018	[37]
3	Glass/AgNW/Chi-ASA	7.88	~	2018	[56]
4	PET/AgNW/GNs	13.36	~	2018	[24]
5	PET/AgNW /PH1000	14.52	<24	2018	[16]
6	Glass/AZO/AgNW /AZO	13.93	~	2018	[57]
7	Glass/AgNW /RLGO	9.62	~	2019	[58]
8	PEN/orthogonal-AgNW/ PH1000	15.18	500	2020	[59]
9	PET/Ag grid /AgNW/PEI-Zn	14.3	~	2021	[33]
10	PET/AgNW/ZnO	8.94	~	2021	[60]
11	PI/AgNW/ITO	11.9	~	2022	[36]

PET. Further improvement on the flexible TC is on the way.

4. Conclusion

In summary, nickel electroplating is observed to improve both oxidization and corrosion resistance of AgNW TCs, and renders it possible for the application in PSCs where highly corrosive material like halide perovskite material is used. An initial PCE of 18.37 % and T_{80} of 432 h have been obtained when using Ni modified AgNW TC as substrate. In more, Ni modification is found to benefit charge transfer and recombination processes, and also the storage-stability of PSCs, which make such AgNW TC possible substrate for PSCs.

Declaration of Competing Interest

The authors declare that they have no known competing financial interests or personal relationships that could have appeared to influence the work reported in this paper.

Data availability

Data will be made available on request.

Acknowledgments

C. Zhou thanks the financial support of the National Scientific Foundation of China (NSFC, No. 61774170) and Hunan Provincial Natural Science Foundation (No. 2020JJ4759), and the Innovation-Driven Project of Central South University (No. 2020CX006). Y. Gao acknowledges support from the National Science Foundation, United States (NSF, DMR-1903962).

Appendix A. Supplementary data

See supplemental information for XRD patterns of AgNW TC (Fig. S1), effect of nickel electroplating time on the optoelectronic properties of AgNW TCs (Fig. S2), adhesion tests (Fig. S3), comparison on the optoelectronic properties of TCs (Fig. S4), cross-sectional images for electrodes (Figure. S5), cross-sectional SEM images of PSCs (Fig. S6), dark JV curves (Fig. S7), low-frequency region Nyquist plots (Fig. S8), equivalent circuits for IS study (Fig. S9), bending test on flexible TCs and typical JV curves of flexible PSCs basing on AgNW TC (Fig. S10). Supplementary data to this article can be found online at https://doi.org/10.1016/j.apsusc.2022.155250.

References

[1] P. Chen, Y. Bai, S. Wang, M. Lyu, J.-H. Yun, L. Wang, In situ growth of 2D perovskite capping layer for stable and efficient perovskite solar cells, Adv. Funct. Mater. 28 (17) (2018) 1706923.
[2] L. Dou, Emerging two-dimensional halide perovskite nanomaterials, J. Mater. Chem. C 5 (43) (2017) 11165–11173.
[3] A.A. Eliwi, M. Malekshahi Byranvand, P. Fassl, M.R. Khan, I.M. Hossain, M. Frericks, S. Ternes, T. Abzieher, J.A. Schwenzer, T. Mayer, J.P. Hofmann, B. S. Richards, U. Lemmer, M. Saliba, U.W. Paetzold, Optimization of SnO2 electron transport layer for efficient planar perovskite solar cells with very low hysteresis, Adv. Mater. 3 (2022) 456–466.
[4] J. Feng, X. Zhu, Z. Yang, X. Zhang, J. Niu, Z. Wang, S. Zuo, S. Priya, S. Liu, D. Yang, Record efficiency stable flexible perovskite solar cell using effective additive assistant strategy, Adv. Mater. 30 (35) (2018) 1801418.
[5] M. Cai, N. Ishida, X. Li, X. Yang, T. Noda, Y. Wu, F. Xie, H. Naito, D. Fujita, L. Han, Control of electrical potential distribution for high-performance perovskite solar cells, Joule 2 (2) (2018) 296–306.
[6] J. Yan, S.L., X. Qiu, H. Chen, K. Li, Y. Yuan, M. Long, B. Yang, Y. Gao, C. Zhou, Accelerated hole-extraction in carbon-electrode based planar perovskite solar cells by moisture-assisted post-annealing, Appl. Phys. Lett. 114 (2019).
[7] C. Wang, L. Guan, D. Zhao, Y. Yu, C.R. Grice, Z. Song, R.A. Awni, J. Chen, J. Wang, X. Zhao, Y. Yan, Water vapor treatment of low-temperature deposited SnO_2 electron selective layers for efficient flexible perovskite solar cells, ACS Energy Lett. 2 (9) (2017) 2118–2124.
[8] A. Kojima, K. Teshima, Y. Shirai, T. Miyasaka, Organometal halide perovskites as visible-light sensitizers for photovoltaic cells, J. Am. Chem. Soc. 131 (17) (2009) 6050–6051.
[9] H. Min, D.Y. Lee, J. Kim, G. Kim, K.S. Lee, J. Kim, M.J. Paik, Y.K. Kim, K.S. Kim, M. G. Kim, T.J. Shin, S. Il Seok, Perovskite solar cells with atomically coherent interlayers on SnO_2 electrodes, Nature 598 (7881) (2021) 444–450.
[10] D. Amgar, S. Aharon, L. Etgar, Inorganic and hybrid organo-metal perovskite nanostructures: synthesis, properties, and applications, Adv. Funct. Mater. 26 (47) (2016) 8576–8593.
[11] Q. Dong, Y. Fang, Y. Shao, P. Mulligan, J. Qiu, L. Cao, J. Huang, Electron-hole diffusion length >175 um in solution-grown $CH_3NH_3PbI_3$ single crystals, Science 347 (6225) (2015) 967–970.
[12] M.A. Green, A. Ho-Baillie, H.J. Snaith, The emergence of perovskite solar cells, Nat. Photonics 8 (7) (2014) 506–514.
[13] C. Wehrenfennig, G.E. Eperon, M.B. Johnston, H.J. Snaith, L.M. Herz, High charge carrier mobilities and lifetimes in organolead trihalide perovskites, Adv. Mater. 26 (10) (2014) 1584–1589.
[14] D. Priante, I. Dursun, M.S. Alias, D. Shi, V.A. Melnikov, T.K. Ng, O.F. Mohammed, O.M. Bakr, B.S. Ooi, The recombination mechanisms leading to amplified spontaneous emission at the true-green wavelength in CH_3NH_3PbBr 3 perovskites, Appl. Phys. Lett. 106 (8) (2015), 081902.
[15] M.A. Najeeb, Z. Ahmad, R.A. Shakoor, A. Alashraf, J. Bhadra, N.J. Al-Thani, S. A. Al-Muhtaseb, A.M.A. Mohamed, Growth of MAPbBr 3 perovskite crystals and its interfacial properties with Al and Ag contacts for perovskite solar cells, Opt. Mater. 73 (2017) 50–55.
[16] J. Wang, X.L. Chen, F.Y. Jiang, Q. Luo, L.P. Zhang, M.X. Tan, M.L. Xie, Y.Q. Li, Y. H. Zhou, W.M. Su, Y.J. Li, C.Q. Ma, Electrochemical corrosion of Ag electrode in the silver grid electrode-based flexible perovskite solar cells and the suppression method, Sol. RRL 2 (9) (2018) 1800118.
[17] Y. Wang, T. Wu, J. Barbaud, W. Kong, D. Cui, H. Chen, X. Yang, L. Han, Stabilizing heterostructures of soft perovskite semiconductors, Science 365 (6454) (2019) 687–691.
[18] S. Wu, R. Chen, S. Zhang, B.H. Babu, Y. Yue, H. Zhu, Z. Yang, C. Chen, W. Chen, Y. Huang, S. Fang, T. Liu, L. Han, W. Chen, A chemically inert bismuth interlayer enhances long-term stability of inverted perovskite solar cells, Nat. Commun. 10 (1) (2019) 1161.
[19] P. Xia, D.E. Guo, S. Lin, S. Liu, H. Huang, D. Kong, Y. Gao, W. Zhang, Y. Hu, C. Zhou, Simultaneous Improvement of the Power Conversion Efficiency and Stability of Perovskite Solar Cells by Doping PMMA Polymer in Spiro-OMeTAD-Based Hole-Transporting Layer, Sol. RRL 5 (11) (2021) 2100408.
[20] S. Liu, D. Zhang, Y. Sheng, W. Zhang, Z. Qin, M. Qin, S. Li, Y. Wang, C. Gao, Q. Wang, Y. Ming, C. Liu, K. Yang, Q. Huang, J. Qi, Q. Gao, K. Chen, Y. Hu, Y. Rong, X. Lu, A. Mei, H. Han, Highly oriented $MAPbI_3$ crystals for efficient hole-conductor-free printable mesoscopic perovskite solar cells, Fundamental Research 2 (2) (2022) 276–283.
[21] T. Shi, S. Lin, M. Fang, D. Kong, Y. Yuan, Y. Gao, B. Yang, H. Han, C. Zhou, Low-temperature fabrication of carbon-electrode based, hole-conductor-free and mesoscopic perovskite solar cells with power conversion efficiency > 12% and storage-stability > 220 days, Appl. Phys. Lett. 117 (16) (2020), 163501.
[22] J. Feng, X. Zhu, Z. Yang, X. Zhang, J. Niu, Z. Wang, S. Zuo, S. Priya, S.F. Liu, D. Yang, Record efficiency stable flexible perovskite solar cell using effective additive assistant strategy, Adv. Mater. 30 (35) (2018) e1801418.
[23] X. Hu, X. Meng, L. Zhang, Y. Zhang, Z. Cai, Z. Huang, M. Su, Y. Wang, M. Li, F. Li, X. Yao, F. Wang, W. Ma, Y. Chen, Y. Song, A mechanically robust conducting polymer network electrode for efficient flexible perovskite solar cells, Joule 3 (9) (2019) 2205–2218.

[24] X. Liu, X. Yang, X. Liu, Y. Zhao, J. Chen, Y. Gu, High efficiency flexible perovskite solar cells using SnO_2/graphene electron selective layer and silver nanowires electrode, Appl. Phys. Lett. 113 (20) (2018), 203903.
[25] Q. Luo, H. Ma, Q. Hou, Y. Li, J. Ren, X. Dai, Z. Yao, Y. Zhou, L. Xiang, H. Du, H. He, N. Wang, K. Jiang, H. Lin, H. Zhang, Z. Guo, All-carbon-electrode-based endurable flexible perovskite solar cells, Adv. Funct. Mater. 28 (11) (2018) 1706777.
[26] D.H. Zhang, R.Q. Liang, Z.K. Liu, H.B. Yang, J.H. Shi, Y.M. Song, D.B. Zhang, A. M. Liu, Research on the interfacial interaction between polyacetylene and silver nanowire, Macromol. Theory Simul. 29 (6) (2020) 2000034.
[27] J. Zhang, X. Hu, H. Li, K. Ji, B. Li, X. Liu, Y. Xiang, P. Hou, C. Liu, Z. Wu, Y. Shen, S. D. Stranks, S.R.P. Silva, H.-M. Cheng, W. Zhang, High-performance ITO-free perovskite solar cells enabled by single-walled carbon nanotube films, Adv. Funct. Mater. 31 (37) (2021) 2104396.
[28] Y.G. Jia, C. Chen, D. Jia, S.X. Li, S.L. Ji, C.H. Ye, Silver nanowire transparent conductive films with high uniformity fabricated via a dynamic heating method, ACS Appl. Mater. Interfaces 8 (15) (2016) 9865–9871.
[29] D. Li, W.Y. Lai, F. Feng, W. Huang, Post-treatment of screen-printed silver nanowire networks for highly conductive flexible transparent films, Adv. Mater. Interfaces 8 (13) (2021) 2100548.
[30] C. Chen, Y. Zhao, W. Wei, J.Q. Tao, G.W. Lei, D. Jia, M.J. Wan, S.X. Li, S.L. Ji, C. H. Ye, Fabrication of silver nanowire transparent conductive films with an ultra-low haze and ultra-high uniformity and their application in transparent electronics, J. Mater. Chem. C 5 (9) (2017) 2240–2246.
[31] X.N. Ho, J.N. Tey, W.J. Liu, C.K. Cheng, J. Wei, Biaxially stretchable silver nanowire transparent conductors, J. Appl. Phys. 113 (4) (2013), 044311.
[32] F. Hoeng, A. Denneulin, G. Krosnicki, J. Bras, Positive impact of cellulose nanofibrils on silver nanowire coatings for transparent conductive films, J. Mater. Chem. C 4 (46) (2016) 10945–10954.
[33] F. Qin, L. Sun, H. Chen, Y. Liu, X. Lu, W. Wang, T. Liu, X. Dong, P. Jiang, Y. Jiang, L. Wang, Y. Zhou, 54 cm^2 large-area flexible organic solar modules with efficiency above 13%, Adv. Mater. 33 (39) (2021) 2103017.
[34] S.P. Hou, J. Liu, F.P. Shi, G.X. Zhao, J.W. Tan, G. Wang, Recent advances in silver nanowires electrodes for flexible organic/perovskite light-emitting diodes, Front. Chem. 10 (2022), 864186.
[35] E. Jung, C. Kim, M. Kim, H. Chae, J.H. Cho, S.M. Cho, Roll-to-roll preparation of silver-nanowire transparent electrode and its application to large-area organic light-emitting diodes, Org. Electron. 41 (2017) 190–197.
[36] R. Miao, P. Li, W. Zhang, X. Feng, L. Qian, J. Fang, W. Song, W. Wang, Highly foldable perovskite solar cells using embedded polyimide/silver nanowires conductive substrates, Adv. Mater. Interfaces 9 (3) (2022) 2101669.
[37] T.-Y. Jin, W. Li, Y.-Q. Li, Y.-X. Luo, Y. Shen, L.-P. Cheng, J.-X. Tang, High-performance flexible perovskite solar cells enabled by low-temperature ALD-assisted surface passivation, Adv. Opt. Mater. 6 (24) (2018) 1801153.
[38] Z. Xiao, Y. Yuan, Y. Shao, Q. Wang, Q. Dong, C. Bi, P. Sharma, A. Gruverman, J. Huang, Giant switchable photovoltaic effect in organometal trihalide perovskite devices, Nat. Mater. 14 (2) (2015) 193–198.
[39] X. Lin, H. Su, S. He, Y. Song, Y. Wang, Z. Qin, Y. Wu, X. Yang, Q. Han, J. Fang, Y. Zhang, H. Segawa, M. Grätzel, L. Han, In situ growth of graphene on both sides of a Cu–Ni alloy electrode for perovskite solar cells with improved stability, Nat. Energy 7 (6) (2022) 520–527.
[40] S. Wang, Y. T, C. Wang, et al., Communication-AgNW networks enhanced by Ni eletroplating for flexible transparent electrodes, J. Electrochem. Soc. 165 (9) (2018) 328–330.
[41] H. Kang, S.-R. Choi, Y.-H. Kim, J.S. Kim, S. Kim, B.-S. An, C.-W. Yang, J.-M. Myoung, T.-W. Lee, J.-G. Kim, J.H. Cho, Electroplated silver-nickel core–shell nanowire network electrodes for highly efficient perovskite nanoparticle light-emitting diodes, ACS Appl. Mater. Interfaces 12 (35) (2020) 39479–39486.
[42] Borensztein, P. De Andres, Monreal, R. Lopez, Flores, Blue shift of the dipolar plasma resonance in small silver particles on an alumina surface, Phys. Rev. B 1986, 33 (4), 2828-2830.
[43] D.E. Guo, J. Ma, S. Lin, X. Guo, H. Huang, D. Kong, F. Xu, Y. Gao, W. Zhang, Y. Hu, C. Zhou, SnO2 modified mesoporous ZrO2 as efficient electron-transport layer for carbon-electrode based, low-temperature mesoscopic perovskite solar cells, Appl. Phys. Lett. 120 (26) (2022), 263502.
[44] G. Yang, C. Chen, F. Yao, Z. Chen, Q. Zhang, X. Zheng, J. Ma, H. Lei, P. Qin, L. Xiong, W. Ke, G. Li, Y. Yan, G. Fang, Effective carrier-concentration tuning of SnO_2 quantum dot electron-selective layers for high-performance planar perovskite solar cells, Adv. Mater. 30 (14) (2018) 1706023.
[45] G. Deignan, I.A. Goldthorpe, The dependence of silver nanowire stability on network composition and processing parameters, Adv. Mater. 7 (57) (2017) 35590–35597.
[46] Z. Yan, H. Chen, M. Li, X. Wen, Y. Yang, W.C.H. Choy, H. Lu, Observing and understanding the corrosion of silver nanowire electrode by precursor reagents and $MAPbI_3$ film in different environmental conditions, Adv. Mater. Interfaces 8 (6) (2021) 2001669.
[47] X. Dong, D. Chen, J. Zhou, Y.-Z. Zheng, X. Tao, High crystallization of a multiple cation perovskite absorber for low-temperature stable ZnO solar cells with high-efficiency of over 20%, Nanoscale 10 (15) (2018) 7218–7227.
[48] J. Song, L. Liu, X.-F. Wang, G. Chen, W. Tian, T. Miyasaka, Highly efficient and stable low-temperature processed ZnO solar cells with triple cation perovskite absorber, J. Mater. Chem. A 5 (26) (2017) 13439–13447.
[49] C. Li, Y. Zhou, L. Wang, Y. Chang, Y. Zong, L. Etgar, G. Cui, N.P. Padture, S. Pang, Methylammonium-mediated evolution of mixed-organic-cation perovskite thin films: a dynamic composition-tuning process, Angew. Chem. Int. Ed. 56 (26) (2017) 7674–7678.
[50] K. Meng, X. Wang, Q. Xu, Z. Li, Z. Liu, L. Wu, Y. Hu, N. Liu, G. Chen, In situ observation of crystallization dynamics and grain orientation in sequential deposition of metal halide perovskites, Front. Chem. 29 (35) (2019) 1902319.
[51] H. Yamada, A.J. Bhattacharyya, J. Maier, Extremely high silver ionic conductivity in composites of silver halide (AgBr, AgI) and mesoporous alumina, Adv. Funct. Mater. 16 (4) (2006) 525–530.
[52] A. Yoshiasa, A. Inaba, T. Ishii, K. Koto, A phase transition of AgI at 150 K, Solid State Ion. 79 (1995) 67–70.
[53] Y. Zhang, J. Wang, J. Xu, W. Chen, D. Zhu, W. Zheng, X. Bao, Efficient inverted planar formamidinium lead iodide perovskite solar cells via a post improved perovskite layer, RSC Adv. 6 (83) (2016) 79952–79957.
[54] Z. Ni, C. Bao, Y. Liu, Q. Jiang, W.-Q. Wu, S. Chen, X. Dai, B. Chen, B. Hartweg, Z. Yu, Z. Holman, J. Huang, Resolving spatial and energetic distributions of trap states in metal halide perovskite solar cells, Science 367 (6484) (2020) 1352–1358.
[55] A. Kim, H. Lee, H.C. Kwon, H.S. Jung, N.G. Park, S. Jeong, J. Moon, Fully solution-processed transparent electrodes based on silver nanowire composites for perovskite solar cells, Nanoscale 8 (12) (2016) 6308–6316.
[56] Y. Jin, Y. Sun, K. Wang, Y. Chen, Z. Liang, Y. Xu, F. Xiao, Long-term stable silver nanowire transparent composite as bottom electrode for perovskite solar cells, Nano Res. 11 (4) (2018) 1998–2011.
[57] E. Lee, J. Ahn, H.-C. Kwon, S. Ma, K. Kim, S. Yun, J. Moon, All-solution-processed silver nanowire window electrode-based flexible perovskite solar cells enabled with amorphous metal oxide protection, Adv. Energy Mater. 8 (9) (2018) 1702182.
[58] H. Chen, M. Li, X. Wen, Y. Yang, D. He, W.C.H. Choy, H. Lu, Enhanced silver nanowire composite window electrode protected by large size graphene oxide sheets for perovskite solar cells, Nanomaterials 9 (2) (2019).
[59] S. Kang, J. Jeong, S. Cho, Y.J. Yoon, S. Park, S. Lim, J.Y. Kim, H. Ko, Ultrathin, lightweight and flexible perovskite solar cells with an excellent power-per-weight performance, J. Mater. Chem. A 7 (3) (2019) 1107–1114.
[60] H. Liu, J. Wu, Y. Fu, B. Wang, Q. Yang, G.D. Sharma, M.L. Keshtov, Z. Xie, One-step solution-processed low surface roughness silver nanowire composite transparent electrode for efficient flexible indium tin oxide-free polymer solar cells, Thin Solid Films 718 (2021), 138486.